

Visible Laser-Induced Nucleation and Growth of Cr, Mo, and W Films from the Hexacarbonyls. Reactivity of CO on Film Surfaces

F. A. Houle*

IBM Research Division, Almaden Research Center, 650 Harry Road, San Jose, California 95120-6099

and K. A. Singmaster*

Department of Chemistry, San Jose State University, San Jose, California 95192 (Received: July 15, 1992; In Final Form: September 25, 1992)

Continuous visible laser irradiation is used to deposit Cr, Mo, and W films from the hexacarbonyls by thermal excitation. Detailed analyses of the films by scanning Auger microscopy show that the Mo and Cr films are spatially inhomogeneous, having clean metal centers surrounded by contaminated metal rings. W films are completely pure. Depth profiles reveal that, prior to formation of clean Mo and Cr, an interfacial layer of contaminated material is deposited which becomes progressively metal rich as thickness increases. If such a layer is formed for W, it is very thin. The measured composition profiles are compared to calculated surface temperature distributions in order to extract information on the kinetics of CO dissociation and desorption during growth. The temperature and mechanism simulations show that CO desorption dominates above about 450 K, ensuring that pure metal is deposited. Below that temperature contamination occurs. Previous investigations of film growth from metal hexacarbonyls have led to the conclusion that film purity will only be high at temperatures exceeding 800 K, where recombinative desorption of CO is fast. The origins of the large discrepancy in temperatures are discussed. Chemical processes leading to growth of metal oxycarbide material at the film edges and film-substrate interface are explored using data from the catalysis literature. The strong parallels found between the laser-deposited material and supported catalysts formed from the hexacarbonyls suggest that the oxycarbide films may have significant Lewis acid-base character, leading to faster CO and metal-CO bond dissociation rates. Thus, formation of contaminated material appears to depend on local surface composition as well as temperature.

Introduction

The identification of useful gas-phase precursors for laser-induced chemical vapor deposition (LCVD) of the early transition metals Cr, Mo, and W has been a surprisingly inactive area. Since the process uses a laser beam to heat a localized area of the substrate and cause pyrolytic decomposition of incident molecules, the few precursor systems which have been studied are those used previously in conventional chemical vapor deposition (CVD) processes. By far, the major effort has been applied to continuous laser deposition from the hexacarbonyl¹⁻⁶ and hexafluoride⁷ of tungsten, with some limited attention to molybdenum hexacarbonyl,^{6,8} chromium hexacarbonyl,^{8,9} and the bis(benzene) complexes of Cr and Mo.¹⁰ Film characterization and process-property data are sparse since the main focus of these investigations has been on rapid direct writing of small features. It has been shown that film resistivities of Mo and W approach those of bulk material as laser power, and thus surface temperatures, increase.⁶ The lowest resistivity reported for W, approximately 1-2 times the bulk value for α -tungsten, is obtained using a 355-nm Ar⁺ laser beam to deposit lines on glass in a cell heated to 360 K.⁶ Surface temperatures are estimated to be 800-1000 K during growth. Although ultraviolet light is used, the photolysis yield of the hexacarbonyls at that wavelength is so small¹¹ that laser heating probably dominates the deposition process, and the results can be compared to visible and infrared laser studies. It might be surmised that low resistivity signals formation of quite pure material, yet separate reports of compositions of films deposited at similar temperatures and cell conditions indicate that purity ranges from "essentially pure"² to having <2% C, <5% O, and 2.5% Si¹ to having 5% C and 20% O.⁴ Similar results are not available for the Mo and Cr hexacarbonyls; films deposited from the bis(benzene) complexes have up to 10% C in them.¹⁰

Additional data on film stoichiometries as a function of temperature are available from the CVD literature for tungsten and molybdenum deposited from the hexacarbonyls in various carrier gases. Similar to findings for LCVD, the film resistivities decrease with increasing temperature, and a minimum temperature of 800 K is found to be necessary for near bulk values to be obtained.¹²

High resistivities are attributed to incorporation of carbon at the lower temperatures. The presence of significant contaminant levels has been confirmed in subsequent studies using preheated gases in reactors at 600-700 K. For example, films of composition $W_{0.25}C_{0.25}O_{0.25}$,¹³ $W_{0.5}C_{0.5}O_{0.25}$,¹⁴ and $Mo_{0.2}C_{0.2}O_{0.2}$ ¹⁵ have been reported. Studies of CVD of chromium films at much lower pressure indicate that this system exhibits similar behavior.¹⁶ Increasing deposition temperature from 550 to 600 K results in a decrease in Cr resistivity from a value about 11 times bulk to 5.5 times bulk. Significant amounts of C and O are seen in the films by Auger spectroscopy, although the concentrations have not been quantified.

The requirement for high temperature to deposit clean films in both LCVD and CVD systems has been attributed to kinetics of CO reactions on the film surfaces. The thermal chemistry of CO on Cr,¹⁷ Mo,¹⁸ and W,¹⁹ $Mo(CO)_6$ on Mo²⁰ and Si,^{20,21} and $W(CO)_6$ on clean and CO-covered W²² and Si^{21,23} has been investigated using a variety of surface spectroscopies. Both the hexacarbonyls and CO desorb quantitatively from Si near room temperature and below; dissociation is not observed.^{20,21,23} In contrast, the reactivity of these molecules with metal surfaces is high. $Mo(CO)_6$ dissociates on polycrystalline Mo above 190 K and is dissociatively chemisorbed at 300 K.²⁰ Similar results have been found for $W(CO)_6$ on W(110)²² and for CO on all three metals.¹⁷⁻¹⁹ Temperature-programmed reaction experiments examining $W(CO)_6$ on tungsten indicate that between 150 and 350 K a fraction of the CO ligands desorb molecularly, with the remainder dissociating to C and O.²² Recombinative desorption of CO does not occur until the surface temperature reaches 800-1000 K. Pure CO dosed onto W(110) displays very similar behavior,^{19,22} as does CO on Mo(110).¹⁸ Competitive desorption and dissociation of CO also occur on Cr(110) near 300 K, but the recombinative desorption path has not been studied because of the instability of the Cr(110) surface at elevated temperature.¹⁷ It is likely that the high-temperature reactions of the CO/Cr system are quite similar to those of CO on W and Mo. On the basis of these data, it has been proposed that clean tungsten films can only be grown at temperatures where recombinative desorption

of CO from the metal surface enables removal of all C and O contaminants at a rate faster than the incorporation rate.²² It is not unreasonable to presume that such considerations apply to the Mo and Cr systems as well.

The usefulness of this proposal rests on the assumption that the kinetic conditions which obtain in a low-coverage, ramped temperature experiment represent well those present during LCVD and CVD where temperature is usually held constant and dosing rates are high. To examine this picture of the deposition process, we have carried out a comprehensive analytical²⁴ and modeling study of thin Cr, Mo, and W films deposited by laser thermal decomposition of the hexacarbonyls. By systematic variation of laser power and deposition time a wide range of surface conditions are accessed. High-resolution scanning Auger microscopy is used to determine film compositions as a function of radial position and depth. The results indicate that there are two clear regimes of growth. The first is a transition regime, involving deposition of contaminated material close to the substrate, clearly observed only for Cr and Mo. The extent of CO dissociation which occurs presents an interesting parallel to the reactivity of supported catalysts. The second is sustained growth of Cr, Mo, or W films which are pure in areas where the surface temperature exceeds a minimum value (estimated to be ≤ 450 K). Thermal modeling of the surface temperature distribution indicates that this minimum is much lower than that determined from CVD and temperature-programmed reaction studies. Kinetic modeling supports the finding that clean metal can be deposited at low temperatures and allows rate coefficients for CO dissociation and desorption during this regime to be estimated. By clarifying the relationship between surface chemistry and temperature and between film composition and stage of growth, the present results allow a more detailed view of the film growth process to be formulated and enable specific areas where understanding is lacking to be identified.

Experimental Section

The experimental methods used in this work are similar to those described in ref 25, except for use of a visible laser beam. Important aspects of the experiments are summarized briefly. All films are deposited on Si(100), doped n- or p-type (10 Ω -cm), cleaned with an acid oxidant bath, and left covered with native oxide to avoid silicide formation during growth. The crystals are attached to large stainless steel sample mounts with stainless steel screws or CuBe spring clips, ensuring uniform heat sinking during the deposition process, and placed in one of two vacuum cells used in this study. After evacuation, the cells are back-filled with neat hexacarbonyl vapors. Cr(CO)₆, Mo(CO)₆, and W(CO)₆ (Aldrich) are placed in small bulbs under dry nitrogen and degassed by three freeze-pump-thaw cycles before each experiment. The cells are at ambient temperature (approximately 293 K) for all experiments. The metal hexacarbonyl vapor pressures are 125 mTorr for Cr(CO)₆, 85 mTorr for Mo(CO)₆, and 19 mTorr for W(CO)₆.

The light source used in most of the experiments is a continuous Ar⁺ laser (Coherent) which provides a Gaussian beam having up to 6 W at 514 nm. A limited number of films have been deposited using relatively high-power frequency-doubled light at 257 nm to compare compositions to those from low-power ultraviolet (UV) light. In all cases the laser beam is expanded with a telescope and focused with a long focal length lens to a 10- μ m spot. Individual circular films are grown with initial incident power densities ranging from 1.5 to 4 MW/cm² and exposure times ranging from 200 ms to 120 s. The first film deposited during each run is typically at 4 MW/cm² for 60 s. This produces a thin layer of material over a >1 -mm² area of the substrate which in our experience (and in agreement with previous studies⁴) is necessary to obtain controlled nucleation of the remaining films. Additional films are grown in a grid at separations of 1 mm.

In order to assess the influence of background gas and air exposure on film compositions, films are grown under all of the following vacuum conditions: low-vacuum cell (10⁻⁴ Torr base pressure) and exposed to air prior to analysis (LV/air), high-vacuum cell ($<10^{-8}$ Torr base pressure) and exposed to air prior to analysis (HV/air), and high-vacuum cell and transferred under

vacuum to the Auger spectrometer (HV/vac). When it occurs, the duration of air exposure is less than 10 min.

All films are analyzed with a PHI 600 scanning Auger multiprobe using a 10-keV electron beam (<10 nA, 200-nm diameter). Survey spectra and linescans are measured for each film before and after sputtering (2-keV Ar⁺, 20–40 $\text{\AA}/\text{min}$). Scanning electron micrographs are obtained with either the PHI system (low resolution) or a Hitachi S-800 scanning electron microscope (high resolution).

Uncertainties in determination of film stoichiometries from the Auger survey data arise from several sources.²⁵ The relative error in repeatability of peak-to-peak height measurements is conservatively estimated from the HV/vac data to be $\pm 30\%$. Reference oxide and carbide standards as well as literature data are used to assist in the determination of stoichiometric ratios and in the assessment of beam damage and preferential sputtering. Complete details are presented in ref 25. If the films had simple monolayer coverages of C and O or if they were pure oxides or carbides, the reference data would be sufficient to obtain accurate compositions for laser-deposited material. Extrapolation to mixed metal oxycarbides adds considerable uncertainty, however, because of the unknown extent of interactive effects such as oxygen-induced broadening of metal Auger transitions with valence band character. This problem is particularly important in the W system. Thus, more weight should be given to trends in the survey data than to absolute compositions. Stoichiometries are valid to one significant figure. Direct comparison of survey data and linescans is not appropriate since linescan data are obtained from signal intensity differences in the integral Auger spectra, while surveys use derivative spectra. Where transitions overlap, such as Cr and O, separation of the two is extremely difficult. Thus, no attempt has been made to quantify the linescan measurements.

Phenomenological deposition rates are obtained for Mo HV/vac films by measuring a series of film heights using an optical microscope. Since the morphology and topography of the films vary significantly with vacuum conditions, the value obtained is only a rough measurement of the deposition rate.

Film Characterization

Physical Aspects. Depending on laser power, deposition time, and cell base pressure, film morphologies and topographies vary widely. In general, the Cr and Mo LV/air films appear smoother than the HV films, while no significant differences are found for W. The films have a general profile of an inner core surrounded by an outer ring. If both grow at the same rate, a smooth disk is obtained (see Figure 1a for Mo). This is observed for all three metals under rather specific conditions: depending on the metal, they fall into the range 2.5–3.1 MW/cm², 1–10-s illumination time. If inner and outer regions do not grow at the same rate, structures such as those presented in Figure 1b,c are formed. The growth of each region need not be concurrent: for example, the Cr films can grow initially as a ring which later fills in or start as a flat structure which eventually is surrounded by a narrow ring. Insufficient data exist to attribute these trends to any particular aspect of the growth conditions; however, it may be significant that Cr LV/air films grow consistently as rings (volcanoes). Mo films, on the other hand, always start as flat disks, then develop a raised ring, and finally grow central domed structures which usually exhibit strong faceting (Figure 1c). Similar trends are found for LV/air films. W films have both types of profiles, being similar to Mo for short illuminations (<30 s) at powers below 4 MW/cm² and more like Cr at higher powers and long illumination times. The latter may be attributable to the fact that high-power density irradiation (4 MW/cm²) leads to damage of the Si substrate as a result of severe laser heating. At these power densities a short exposure time (200 ms) results in the formation of a rippled structure of about 500-nm spatial frequency on the Si substrate. These structures indicate that the substrate has melted as film growth begins.²⁶

Charging upon exposure to the electron beam is only observed for Cr films deposited under LV/air conditions. This is consistent with analytical data presented below which show that these are

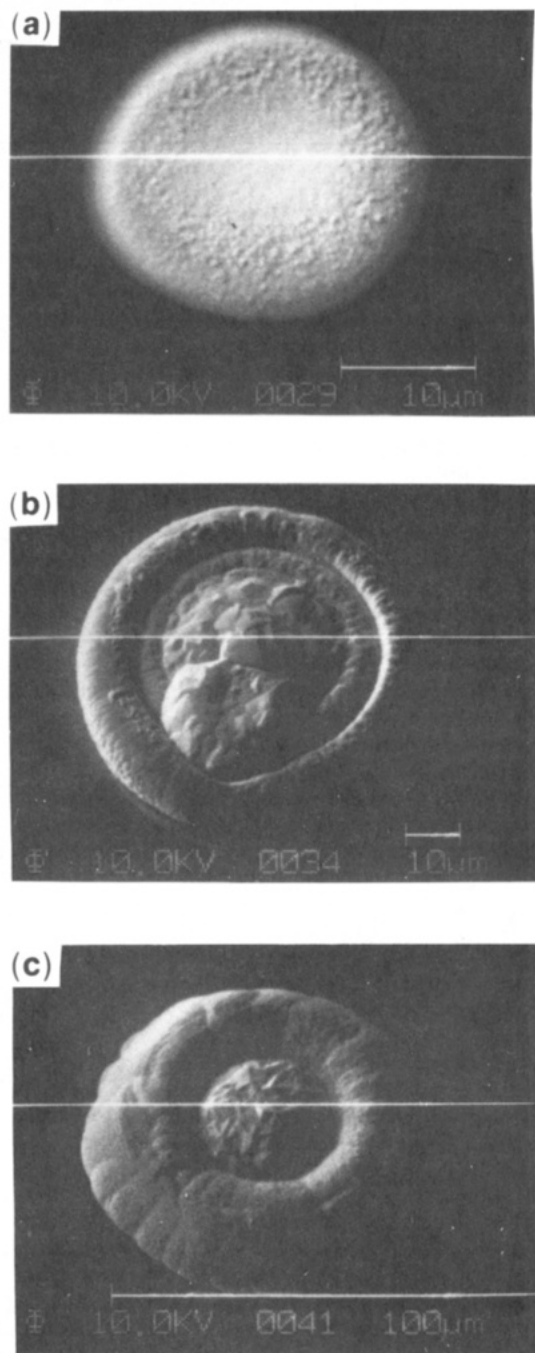


Figure 1. Scanning electron micrographs of films deposited from Mo(CO)₆ using CW visible laser irradiation (HV/vac): (a) 2.5 MW/cm², 1 s; (b) 2.0 MW/cm², 30 s; (c) 1.5 MW/cm², 60 s.

the only films which grow as oxides.

Deposition Rates. Due to the varied topography of the films, it is difficult to obtain a meaningful measurement of deposition rates for the conditions used. An attempt to do so for the Mo HV/vac films resulted in rates ranging from 2000 to 6000 Å/s. Perhaps a more useful way of comparing rates among the metals, and thus gaining some appreciation for ease of film formation, is to compare film diameters determined from linescan data of briefly sputtered films as a function of laser power density and deposition time. Although films are pre-nucleated for all three as described in the Experimental Section, W films reach 15–20- μm diameter after 10 s of illumination of 2.3–2.8 MW/cm², while Cr and Mo reach diameters of 20–30 μm using similar power densities after 1 s or less. At early times (10 s or less) the Mo films tend to be of the order of 25% wider than those of Cr, while later (30 s) they are nearly equal (e.g., 90 μm for Mo at 2 MW/cm², 70 μm for Cr at 1.8 MW/cm²). After 30 s at these power densities the W films are 10–20 μm in diameter. The W

films do not always remain small, however. At 2.8 W/cm², after slowly increasing to 60 μm for 90 s, the width of the films grows rapidly to 150 μm after 4-min illumination. The outer 45- μm wide ring is easily oxidized, indicating it is much less dense than the central part of the film. This suggests that the W system has stringent requirements for surface temperature and irradiation time to initiate and sustain growth. Assuming the differences in film diameter reflect growth rate, the much smaller W films may be attributable in part to the low vapor pressure of W(CO)₆ compared to those of Mo(CO)₆ and Cr(CO)₆. Surface chemical factors may also be important; they are discussed later in the paper.

Film Compositions. The intrinsic composition of material deposited by 514-nm irradiation of an absorbing substrate through nonabsorbing hexacarbonyl vapor is obtained by examination of films deposited in high vacuum and analyzed without exposure to air (HV/vac). HV/air films (deposited in high vacuum, exposed to air) provide information on the changes these materials undergo in air. The LV/air films (deposited in low vacuum, exposed to air) reveal the effect of oxygen-containing background gases present in the deposition cell on film compositions.

Spatially resolved Auger surveys are obtained for all films in order to establish stoichiometries at selected locations on film surfaces and within their bulk. Linescans measured for HV/vac films provide information on the radial dependence of film compositions. Tables I–IV list the elemental compositions as well as peak-to-peak height ratios obtained from survey data for Cr, Mo, and W films deposited under various conditions. Peak-to-peak height ratios are calculated using the following transitions: O (KLL, 503 eV), C (KLL, 272 eV), Cr (LMM, 529 eV), Mo (MNN, 186 eV), and W (MNN, 1736 eV). The percent compositions correspond to the average values and are provided for the purpose of comparison to previous studies. Also included are the predicted values for certain metal–carbon–oxygen stoichiometries calculated from Auger electron sensitivities at 10 keV²⁷ and experimentally determined ratios for refractory metal oxides and carbide powders (Aldrich) imbedded in In foil.²⁵

Each entry in Tables I–IV combines data from 12 to 45 individual films except for the off-spot entries where only 3–5 regions are included. The data are organized as follows. Compositions are reported for film surfaces (unsputtered) and film bulk (sputtered). The data show no significant variation in composition over the laser power density range used, so results for all intensities are combined. With the exception of a few very thin deposits, film compositions do not vary with deposition time, so data for all times are merged in the tables. Metal-containing material is observed at distances far removed from the films (2 mm for a high-power, long-exposure film) as well as between pairs of films. This off-spot composition is obtained for HV/vac substrates and is listed in Tables I, II, and IV. The thickness of the off-spot deposit depends on the distance from the spot and sometimes is thick enough to be sputtered (>100 Å). Film compositions are found to be spatially inhomogeneous so data for film centers and edges are listed separately. Film compositions remain constant through most of the bulk after the initial 10–20-Å film surface region is removed, changing only near the substrate. Accordingly, sputtered film data correspond to depths ranging from 60 to 1000 Å.

Cr Films. The data in Table I indicate that the surface composition (unsputtered) of edges and centers for both HV/vac and HV/air films is surprisingly uniform, roughly consistent with a CrCO stoichiometry. As can be seen in Figures 2 and 3, the Auger line shapes for carbon indicate that it is graphitic or amorphous.²⁸ The surface layer is removed within the first 1–2 min of sputtering, corresponding to a thickness of less than 50 Å. This surface material may result from additional decomposition of gas-phase hexacarbonyl after irradiation is complete. The off-spot material has considerably more C and O in it, consistent with an approximate stoichiometry of CrC₂O₂.

Once the HV films are sputtered, significant reductions in C and O content are observed for the film centers. The low signal levels make determination of the chemical state of the carbon difficult to assess, but it does appear to have more carbidic

TABLE I: Compositions of Cr Films Deposited from $\text{Cr}(\text{CO})_6$ by CW Ar^+ Laser

films	Auger data				% composition		
	average		range		O	C	Cr
	C/Cr	O/Cr	C/Cr	O/Cr			
unspattered							
center							
LV/air	0.10	2.9	0.0-0.20	2.3-3.3	63	10	27
HV/air	0.22	1.5	0.10-0.49	0.9-2.3	40	26	34
HV/vac	0.23	1.6	0.13-0.40	0.8-2.3	42	26	32
edge							
LV/air	0.11	2.8	0.0-0.30	2.4-4.1	62	11	27
HV/air	0.26	1.6	0.12-0.43	1.1-2.4	44	32	34
HV/vac	0.23	1.6	0.15-0.30	1.3-2.1	42	26	32
off spot	0.53	3.1	0.30-0.90	2.6-3.8	46	35	19
sputtered							
center							
LV/air	0.00	2.3	0	1.9-2.7	65	0 ^a	35
HV/air	0.07	0.2	0.0-0.20	0.0-0.5	12	18	70
HV/vac	0.00	0.3	0.0-0.05	0.1-0.6	18	5	76
edge							
LV/air	0.00	2.4	0	2.1-2.7	67	0 ^a	33
HV/air	0.26	0.4	0.10-0.40	0.2-0.8	14	41	45
HV/vac	0.08	0.8	0.0-0.10	0.5-1.1	33	15	52
standards							
Cr_2O_3							
unspat		2.4	2.4-2.5		65		35
sput		2.0	1.9-2.0		61		39
predicted							
Cr_2O_3			1.9		60		40
CrCO		0.28	1.2		33	33	33
CrC_2O_2		0.57	2.4		40	40	20

^a Below the limit of detection.

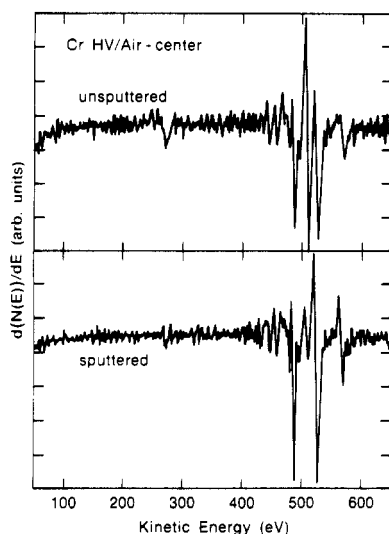


Figure 2. Auger survey spectra of an HV/air Cr film deposited using a 2.65 MW/cm² beam for 30 s.

character than the surface carbon.²⁸ Figures 2 and 3 present typical spectra for air-exposed and vacuum-transferred films. Although the average composition for these films indicates the presence of O and, rarely, C in the film centers, on some occasions carbon- and oxygen-free spectra were observed (Figure 4). These results are incorporated into the range data in Table I. To our knowledge, this is the first time clean Cr been deposited by any type of laser-assisted process. This result indicates that complete removal of CO from the growing film can be accomplished, at least in the film centers. The occasional varying levels of oxygen detected in film centers, particularly those of HV/vac films, is most likely a result of scavenging of background gas during deposition. This effect is most pronounced in the LV/air films, which grow as Cr_2O_3 .

The sputtered edges of both HV/air and HV/vac films have higher levels of C and O than the centers. This is not surprising: since the deposition process is thermally driven, the decrease in temperature as a function of distance from the laser beam center

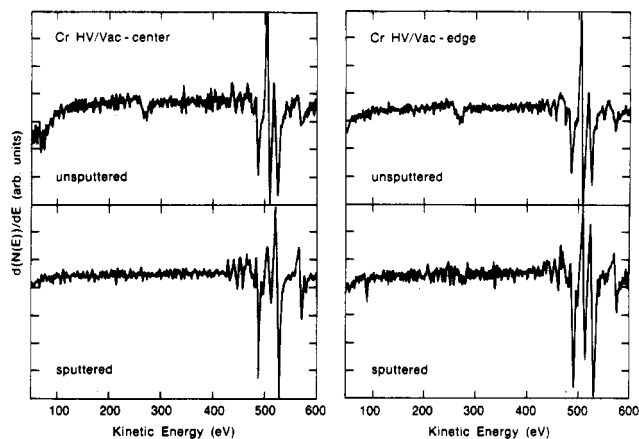


Figure 3. Auger survey spectra of an HV/vac Cr film deposited using a 2.6 MW/cm² beam for 30 s. The small Si signal in the sputtered film edge spectrum is from overlap of the electron beam raster pattern with a small area of the substrate.

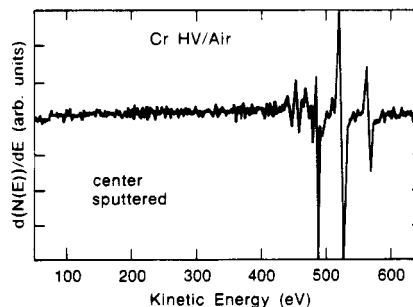


Figure 4. Auger survey spectrum of an HV/air Cr film deposited using a 2.55 MW/cm² beam for 10 s. Carbon (272 eV) and O (503 eV) are absent.

can strongly influence the surface chemistry during film growth. Radial profiles of these impurities are obtained by Auger linescans. It should be noted that although linescans provide a way of visualizing spatial distributions of elements, they should not be

TABLE II: Compositions of Mo Films Deposited from Mo(CO)₆ by CW Ar⁺ Laser

films	Auger data				% composition		
	average		range		O	C	Mo
	C/Mo	O/Mo	C/Mo	O/Mo			
unspattered							
center							
LV/air	0.31	2.8	0.20-0.50	1.6-4.3	49	24	27
HV/air	0.77	2.1	0.40-1.20	1.2-3.5	30	48	22
HV/vac	0.46	1.2	0.34-0.65	0.8-1.6	25	43	32
edge							
LV/air	0.35	3.0	0.20-0.50	1.8-4.3	50	25	25
HV/air	0.73	2.0	0.40-1.00	1.1-2.9	30	48	22
HV/vac	0.58	1.4	0.31-0.87	1.0-1.9	26	47	28
off spot	0.97	2.1	0.80-1.40	1.8-2.6	27	54	19
sputtered							
center							
LV/air	0.0	0.2	0.0-0.10	0.1-0.4	13	0 ^a	87
HV/air	0.0	0.0	0.0-0.20	0.0-0.3	0 ^a	0 ^a	100
HV/vac	0.0	0.0	0	0	0 ^a	0 ^a	100
edge							
LV/air	0.0	0.4	0	0.3-0.7	23	0 ^a	77
HV/air	0.15	0.2	0.0-0.30	0.0-0.4	9	28	63
HV/vac	0.10	0.2	0.0-0.23	0.0-0.4	8	21	71
off spot	0.32	0.4	0.27-0.35	0.3-0.6	12	43	45
standards							
MoO ₃							
unspat		5.7		5.0-6.0	76		21
sput		3.4		3.0-3.8	69		31
predicted			4.5		75		25
MoO ₃							
MoC		0.34				50	50
MoCO		0.34	1.5		33	33	33
MoC ₂ O ₂		0.68	3.0		40	40	20

^a Below the limit of detection.

TABLE III: Compositions of Mo Films Deposited from Mo(CO)₆ at 257 nm (HV/vac)

films	Auger data				% composition		
	average		range		O	C	Mo
	C/Mo	O/Mo	C/Mo	O/Mo			
unspattered							
low power ^a	0.63	1.5	0.53-0.74	1.0-1.9	27	46	27
high power	0.81	1.9	0.63-1.12	1.6-2.2	27	51	22
sputtered							
low power ^a	0.59	0.8	0.50-0.70	0.6-1.0	16	53	30
high power	0.52	0.6	0.28-0.63	0.3-0.8	14	52	34

^a Reference 25.

directly used to determine stoichiometries since the sensitivities are uncalibrated and, for the case of Cr in particular, the Cr and O peaks overlap. A linescan-sputtering sequence for a HV/vac Cr film is illustrated in Figure 5, starting after removal of the surface material. The top two panels are similar, indicating that the bulk of the film is homogeneous to a radius of about 10 μm, at which point C and O levels rise abruptly. The annular contaminated region is about 2-4 μm wide. The last linescan in the sequence shows that the carbon profile is extended into the center of the film, indicating that at early times the fraction of the deposited material which is contaminated is significantly greater and the carbon and oxygen concentrations are higher. This phenomenon is observed under two conditions: long sputter times for thick deposits and at all sputter depths in very thin deposits. Survey data taken at the centers of two films show an average C/Cr ratio of 0.21 (range 0.15-0.28) and O/Cr ratio of 0.60 (range 0.48-0.66). These values are consistent with a stoichiometry of CrC_{0.7}O_{0.5}, showing that oxygen and carbon concentrations are much lower than in the unspattered off-spot layer. Thus, it appears that at the initial stages of growth the film formed is an oxycarbide. The nonuniformity of the profile and its distinct composition show that the material is not the ubiquitous off-spot layer, but has been deposited on top of it.

Mo Films. Data in Table II show that, unlike Cr, the surface compositions of the unspattered Mo films vary strongly with

vacuum conditions. This material, which is radially uniform and is removed in the first 1-3 min of sputtering, probably originates from surface reactions on the film after the irradiation has been terminated and is further oxidized by air exposure. Its composition, given by HV/vac data, is roughly consistent with a MoC₂O stoichiometry. The Auger line shapes presented in Figures 6-8 indicate that the surface carbon is amorphous or graphitic.²⁹

As shown in Table II and in Figures 6-8, once the films are sputtered the levels of C and O impurities are drastically reduced regardless of deposition conditions. This is not a result of preferential sputtering of oxygen, as was observed in the case of photochemical deposition from Mo(CO)₆.²⁵ In that case the reduction was gradual (over 10 min of sputter time), eventually reaching a steady level. Complete loss of oxygen could not be obtained from the photochemical films or from MoO₃ standards by sputtering for periods as long as 80 min. Under identical electron beam and sputtering conditions the films deposited with 514-nm light reach their stable composition within 1-3 min, remaining constant until material close to the substrate is reached. This is a strong indication that the elemental compositions listed for sputtered films reflect actual film compositions and not an artifact. Therefore, the centers of the HV/vac films are pure Mo, with upper limits of 2% C and 1% for O, as given by the detection limits of Auger electron spectroscopy. Typical Auger survey data are shown in Figure 8. Clean centers are usually observed for

TABLE IV: Compositions of W Films Deposited from $W(CO)_6$ by CW Ar⁺ Laser

films	Auger data				% composition		
	average		range		O	C	W
	C/W	O/W	C/W	O/W			
unspattered							
center							
LV/air	0.31	1.9	0.28–0.43	1.1–3.9	25	18	57
HV/air	0.37	1.4	0.20–0.60	0.9–2.6	19	22	59
HV/vac	0.44	1.8	0.26–0.59	1.1–3.0	22	24	53
edge							
LV/air	0.33	2.9	0.28–0.45	1.9–4.1	34	17	50
HV/air	0.44	1.8	0.30–1.00	1.2–3.0	22	24	53
HV/vac	0.47	1.8	0.39–0.56	1.0–2.6	22	25	53
off spot	0.85	3.8	0.69–1.11	3.1–5.1	32	32	36
sputtered							
center							
LV/air	0.0	0.2	0	0.0–0.8	4	0 ^a	96
HV/air	0.0	0.0	0	0	0 ^a	0 ^a	100
HV/vac	0.0	0.0	0	0	0 ^a	0 ^a	100
edge							
LV/air	0.0	0.8	0	0.0–0.8	16	0 ^a	84
HV/air	0.0	0.0	0	0.0–0.1	0 ^a	0 ^a	100
HV/vac	0.0	0.0	0	0.0–0.3	0 ^a	0 ^a	100
standards							
WC							
unspat	1.0		1.1–0.9			50	50
sput	1.2		1.4–0.9			55	45
WO ₃							
unspat		6.4		5.4–6.9	60		40
sput		3.8		3.0–4.0	43		57
predicted							
WC	1.0					50	50
WO ₃		12.8			75		25
WCO	1.0	4.3			33	33	33
WC ₂ O ₂	2.0	8.6			40	40	20

^a Below the limit of detection.

HV/air films (Figure 7) as well, although a few films did show traces of O. The fact that HV/vac and HV/air films are remarkably similar in composition indicates that the films can tolerate 5 min of air exposure without significant contamination. This provides evidence that the films are much more dense and impermeable than the photochemically deposited Mo films.²⁵

Data in Table II and Figures 6–8 indicate that once the films are sputtered there are differences in composition as a function of distance from the film center. Figure 9 shows a typical bulk linescan for a Mo film after sputtering. As found for the Cr films, C and O are detected in an annular region at the film edge. The Auger line shape shows the carbon to be carbide, rather than amorphous or graphitic as found on the surface.²⁹ The diameter of the pure metal region of the film is significantly larger than the 10- μ m laser beam diameter. Figure 10 shows a linescan for a film deposited at the same power density as that in Figure 9, but with a 1-s exposure time. After the first few minutes of sputtering this film has a radial profile similar to the one shown in Figure 9. As sputtering continues and the material near the substrate is reached, the C and O impurities extend into the center of the film. Survey data for two film centers show that the average Auger intensities are C/Mo = 0.18 (range 0.15–0.21) and O/Mo = 0.25 (0.2–0.3). These data indicate that the early growth material is chemically distinct from the off-spot material.

The off-spot layer, which is analyzed far from illuminated areas and is initialized when the first spot on a given substrate is deposited, serves as a nucleation surface for all films except the first. Its composition is given in Table II, and typical survey spectra are shown in Figure 11. The surface composition of this material is roughly consistent with a stoichiometry of MoC₃O. After sputtering the thicker regions for a few minutes to remove about 100 Å, the oxygen signal is significantly lower. The loss is too large to be attributed solely to preferential sputtering of oxygen.²⁵ This indicates that the layer has a range of compositions. In all cases less oxygen is observed in sputtered material than unspattered material, placing an upper limit of oxygen content to a little above one atom per Mo atom. Since C concentrations are not affected

by sputtering, the data indicate that there is one carbon atom per Mo atom. This result suggests that the nucleation layer close to the Si substrate has an approximate composition MoCO_{<1}.

Both unspattered and sputtered LV/air films are significantly more contaminated than their HV counterparts. Higher levels of oxygen may originate from background gas incorporation during deposition and air exposure.

In an attempt to learn how simultaneous heating might affect the compositions of photochemically deposited films, determined previously²⁵ to be approximately MoC₂O, an HV/vac run for Mo(CO)₆ was also performed using 257-nm irradiation at an initial power density of 0.7 MW/cm² (200 times greater than that used in ref 25). Unfortunately, window deposits significantly attenuated the beam so the extent of heating was not as large as hoped. Data are presented in Table III. Only film centers are analyzed. The films' surface and bulk contain large amounts of oxygen and carbon impurities. For the purpose of comparison we have also included data for low-power UV laser deposition from ref 25. Although the averages for both UV runs are very similar, the ranges of values for high-power density UV deposition are systematically lower than those found at low power. This suggests that high power does tend to reduce contamination, presumably by heating, but the data are not clear-cut. The overall similarity between the UV data sets indicates that both are dominated by photochemical reactions.

W Films. Table IV presents a summary of data for W films deposited under the three different vacuum conditions. Surface compositions are spatially homogeneous and, in the case of HV/vac and HV/air films, roughly consistent with less than one CO group per W. The Auger line shapes for carbon shown in Figures 12–14 indicate that it is primarily graphitic or amorphous on LV/air films but possibly a mixture of graphitic or amorphous and carbide on high-vacuum-deposited films.³⁰ This surface layer, which is not appreciably air sensitive, is probably formed by surface reactions after irradiation is complete. It is removed by 1–3 min of sputtering, indicating that its thickness is of the order of 50 Å. Off-spot material is also observed for W films; however, it

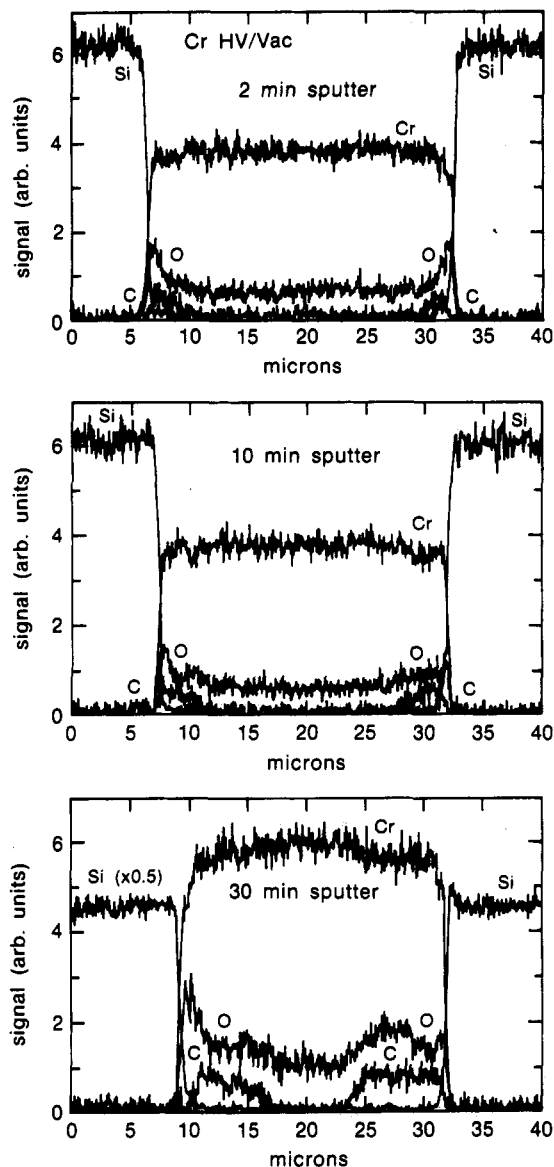


Figure 5. Auger linescans of an HV/vac Cr film deposited using a 2.10 MW/cm² beam for 5 s. Three sputter depths are shown.

is too thin to sputter reliably. The surface composition of this material provides an upper limit to its stoichiometry, approximately WCO.

The high purity of the sputtered films is surprising. For all three vacuum conditions carbon levels are below the detection limit of Auger spectroscopy (<2%). Only traces of oxygen are observed in LV/air films. Although tungsten oxides, like molybdenum, reduce under ion bombardment, the rapid decrease in oxygen signal during the first 1–3 min of sputtering indicates that the lack of measurable contamination is not an artifact. The survey data (Figures 12–14) show clearly that, unlike Mo and Cr, the W film centers and edges have the same compositions. Linescan data presented in Figure 15 confirm the absence of C and O throughout the film. In further contrast to results for Cr and Mo, a region of contaminated material extending into the center is not observed as the films are sputtered down to the substrate.

Simulations

The composition profiles determined by Auger spectroscopy show that Cr and Mo films have clean centers surrounded by annular regions containing metal, carbon, and oxygen. W films are clean across their entire span. Since all films are deposited using a Gaussian laser beam, a well-defined temperature gradient is present at the film surface and the transition from clean to contaminated material must occur over a specific temperature range. Knowledge of this temperature is critical to obtaining an

accurate description of deposition chemistry from the hexacarbonyl precursors. Direct measurements of temperature and surface coverages during film growth are, unfortunately, not feasible for such small surface areas. Therefore, stochastic simulations of surface temperatures and the temperature-dependent reaction mechanism have been performed to gain new insight to LCVD kinetics from the film composition data.

Temperature Distribution Calculations. Radial temperature profiles for conditions corresponding to steady-state film growth have been calculated. It is particularly important that fully temperature-dependent thermal properties of both the film and the substrate are used since an accurate description of the surface temperature distribution is required to quantify the CO incorporation kinetics. This requirement is difficult to meet for layered structures using deterministic methods, and in general approximations are made to the true temperature dependences of properties such as heat capacity and thermal conductivity to make the equations tractable.³¹ For the purposes of the present study, a stochastic approach to calculating heat flow has been used instead.³² Stochastic methods have been shown to be rigorously accurate for simulating the time-dependent properties and behavior of physical systems.³³ They are probabilistic and are relatively easy to implement since the calculations involve mostly simple arithmetic.

The model constructed for this work consists of a volume of space which is broken into a grid of 361 cells identified as either film, substrate, or vacuum depending on location, thus describing a structure with a small film on top of a large substrate. The top layer of cells—belonging to the film in this case—is assumed to absorb laser light according to its wavelength-dependent reflectivity. The light is converted entirely to heat, and the heat is allowed to flow among the film and substrate cells according to the temperature-dependent thermal conductivity of the materials. The instantaneous heat content of a cell is used to determine its temperature using the density of the material and its temperature-dependent heat capacity. Since each cell is presumed to have uniform temperature, the dimensions of the cell provide error limits for the spatial distributions. To simulate heating by a laser beam, the geometry is chosen to be cylindrically symmetric, with a nonuniform grid expanding continuously in both the radial and the vertical directions. The density of cells in the region near to that illuminated by the laser beam is high, allowing temperature gradients to be simulated accurately, while remote cells are large to allow the large size of the substrate and its heat-sinking mounting to be properly described. A useful feature of stochastic simulations is that a single program can be used to simulate a wide variety of laser heating problems with suitable materials and laser beam characteristics provided as input. The code used in the present study has been tested against highly accurate, detailed conventional calculations for CW laser heating of silicon³⁴ and pulsed heating of silver³⁵ and has been found to be in excellent agreement with them. The parameters used for the simulations and results of the calculations are as follows.

Geometry. Deposited films are found to grow radially as well as vertically with time, with development of complex structures (see Figure 1 and Physical Aspects section). It is clear that a single simulation geometry will not be adequate for the full dynamic range of heated films. Since the purpose of the calculations is for comparison to chemical profiles of the films, and similar compositions are found for films whose deposition times exceed about 1 s, only data from 10-s growth times have been modeled. (In several instances, 5- and 30-s data were used when 10-s data were unavailable.) The structures at 10 s are typically of uniform thickness, allowing the simple geometry of a disk on a flat substrate to be assumed. The Cr films have diameters of 20–30 μm and C-free center regions of 10–20 μm. A single diameter of 25 μm is chosen to represent them. Although oxygen contamination of the films by background gases during deposition in high vacuum occurs about half the time, the oxygen levels are assumed to be insufficient to markedly change the optical and thermal properties of the chromium. Mo films are much larger, with diameters ranging from 40 to 45 μm (approximated by 39.5 μm) and clean

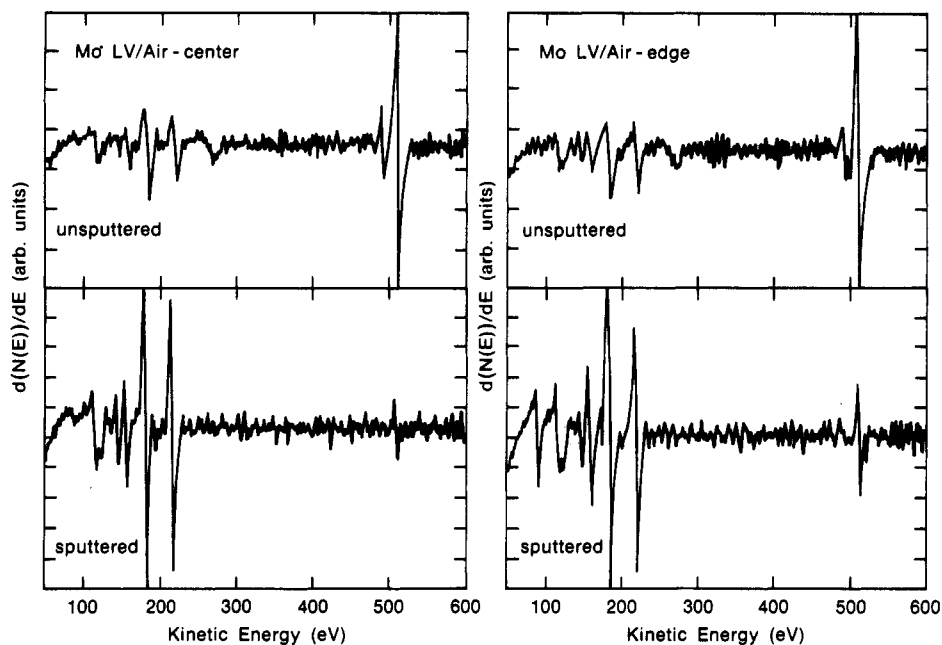


Figure 6. Auger survey spectra of an LV/air Mo film deposited using a 2.60 MW/cm² beam for 30 s.

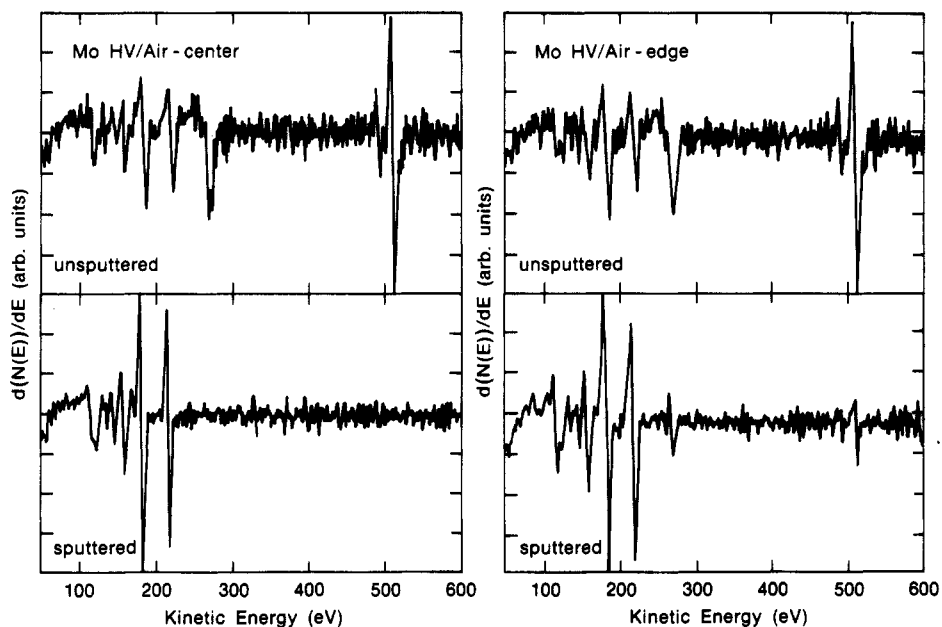


Figure 7. Auger survey spectra of an HV/air Mo film deposited using a 2.55 MW/cm² beam for 30 s.

regions of 30- μm diameter. Although the conditions under which W films will grow are restricted, when they do grow they are found to be pure everywhere. Experimental diameters of 15 and 20 μm are used. All films are assumed to be 2.75 μm thick, a reasonable value. The calculated surface temperatures are not found to be very sensitive to this assumption: heat is redistributed rapidly throughout the metal film and transferred relatively slowly to the silicon because of the large differences in their thermal conductivities. The silicon substrate is a disk 0.547 mm in diameter and 0.534 mm thick. It is found that for the time scale of the simulations (typically $(1-3) \times 10^{-5}$ s) this approximates well a heat-sunk, 1-cm², 0.245-mm-thick wafer. The calculated surface temperature, specifically of interest here, reaches steady state within 1–2 μs in all three systems at all incident powers.

Materials Properties. Although the Cr and Mo films are not found to be radially uniform in composition, they are assumed to be so for the purposes of the simulations since materials information is generally unavailable for mixed nonstoichiometric metal oxycarbides. The thermal conductivities and heat capacities for bulk Cr, Mo, and W over a temperature range 200–1200 K are taken from tabulated values^{36,37} and fit to polynomials. Data

for the thermal conductivity of silicon are handled in a similar way.³⁸ A published expansion for the temperature-dependent heat capacity of silicon³⁹ is used.

Optical Data. The laser beam is assumed to be continuous, with a Gaussian profile and $1/e^2$ diameter of 10 μm . Incident powers are chosen to correspond to experiment, ranging from 1.2 to 3.1 W. Since all the light is absorbed in the top 0.5- μm thick layer of metal film cells, the absorptivity is determined from reflectance data. Bulk reflectivities at 514.5 nm for W (0.493) and Mo (0.594)⁴⁰ and at 512.3 nm for Cr (0.677)⁴¹ are used. Although it is expected to be important, the temperature dependence of the optical data is not included since it is unavailable. The reflectivity of most metals increases with temperature, so the use of a constant value results in an overestimation of the rate of energy input to the films.

Calculated Distributions. The results of the simulations are presented in Figure 16. The temperatures of the top layer of cells belonging to the metal films are shown, with the cell widths and locations of the film edges indicated on the figure. The steady-state temperature profiles are drawn through the centers of the cells. The similarity in temperature distributions for the three metals

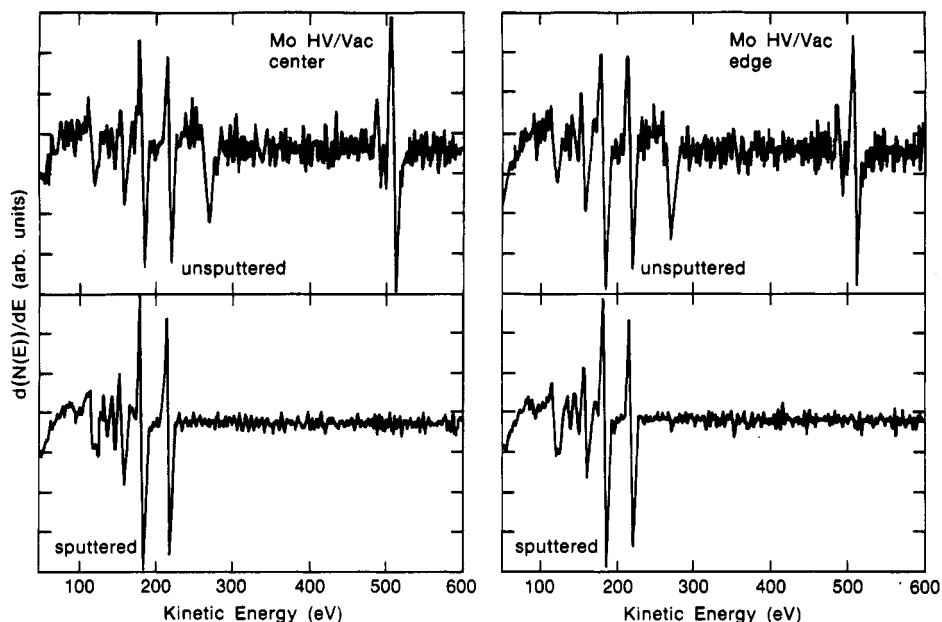


Figure 8. Auger survey spectra of an HV/vac Mo film deposited using a 2.55 MW/cm^2 beam for 10 s.

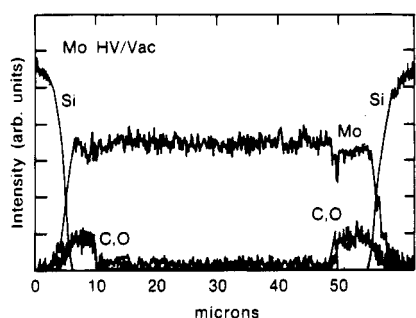


Figure 9. Auger linescan of a Mo film deposited under HV/vac conditions after sputtering for 30 min (2.55 MW/cm^2 , 10 s).

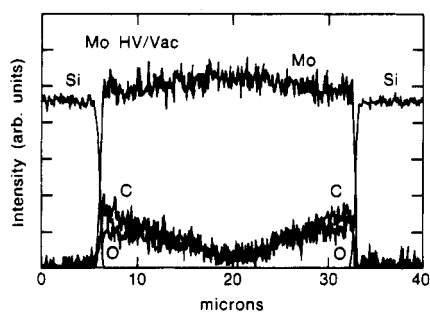


Figure 10. Auger linescan of a Mo film deposited under HV/vac conditions after sputtering for 20 min (2.55 MW/cm^2 , 1 s).

at similar incident power densities reflects opposing trends in decreasing reflectivity and increasing thermal conductivity for the Cr-Mo-W series. Also noted in the figure are the locations of the transition between clean and contaminated regions for each material as determined from the Auger linescans. An upper limit to the surface temperature range corresponding to this transition is denoted by the shaded regions. It is similar for Cr and Mo, indicating that growth of clean metal is expected above 400–450 K. This suggests that desorption of CO from the surface of the growing film is quantitative at and above this temperature range, while competition between desorption and dissociation occurs below it.

Isothermal Reaction Simulations. Mechanistic simulations using kinetic parameters from the literature have been made to provide an independent assessment of the temperature dependence of CO dissociation and incorporation into the growing films. The details of decomposition of the hexacarbonyls on metals are poorly understood,^{20,22} so the steps for release of CO from an adsorbed metal carbonyl complex are treated in only a general way. All three

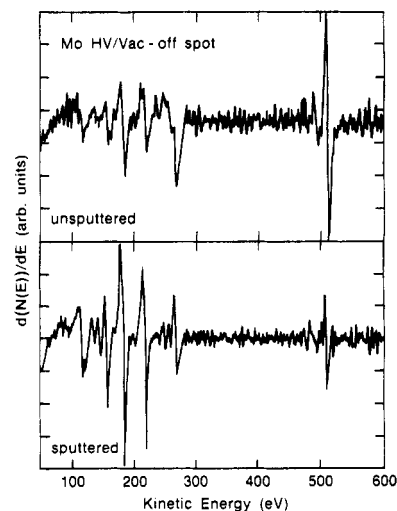


Figure 11. Auger survey spectrum of material deposited in between Mo film spots, HV/vac conditions.

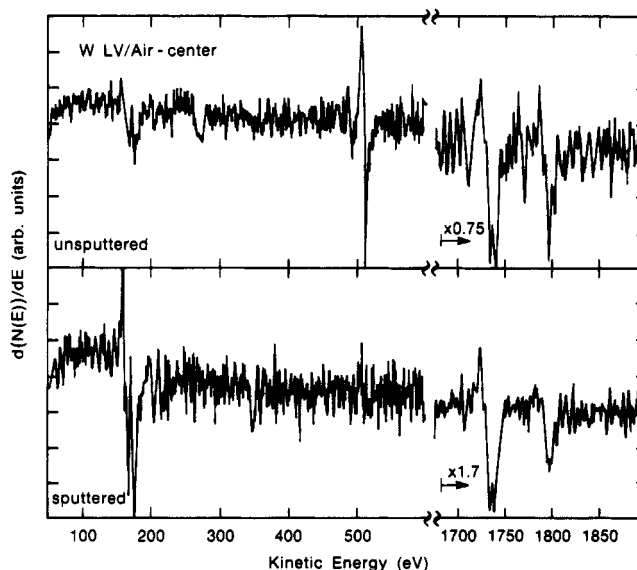


Figure 12. Auger survey spectra of an LV/air W film deposited using a 2.75 MW/cm^2 beam for 60 s.

metals are assumed to have the same kinetics and are designated as M. To simulate a worse case, all six COs are deposited si-

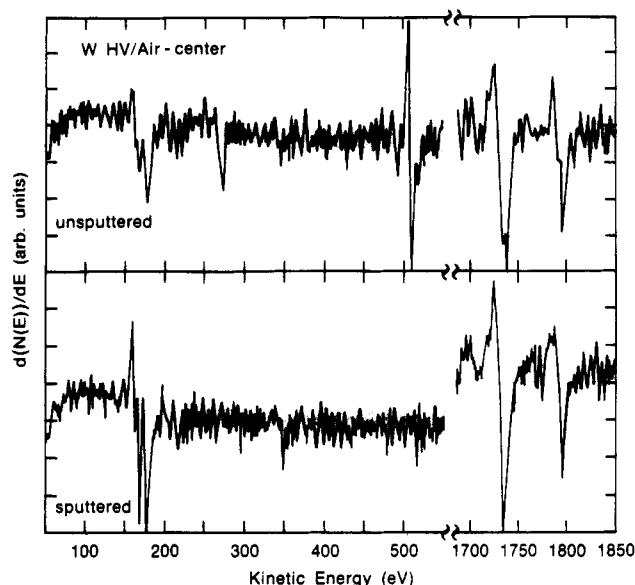
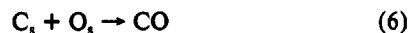
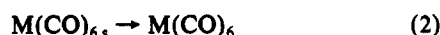


Figure 13. Auger survey spectra of an HV/air W film deposited using a 2.80 MW/cm² beam for 60 s.

multaneously on the surface following dissociation of the precursor. The specific reactions involving CO are considered in greater detail (although they do not include fine points of binding site and orientation differences¹⁷⁻¹⁹) and are explicitly modeled as primary steps.

The mechanism is assumed to be



where the subscript *s* designates a species bound to the surface. In step 1 the metal carbonyl is dosed continuously on the surface, with an impingement rate of $3.9 \times 10^{19} \text{ cm}^{-2} \text{ s}^{-1}$. It can desorb as shown in (2), with an Arrhenius *A* factor and activation energy estimated to be $1 \times 10^{14} \text{ s}^{-1}$ and 12 kcal/mol, respectively. These

values are typical for physisorbed molecules with a high accommodation coefficient, and, if in error, lead to a sticking probability which is too high.⁴² The dissociation of $\text{M}(\text{CO})_{6,s}$ in (3) is not likely to be an elementary step,⁴³ but for the purposes of this model it is assumed that the kinetics of loss of one CO determine the rate of dissociation of the entire complex. The *A* factor is taken to be $1 \times 10^{15} \text{ s}^{-1}$ from gas-phase measurements,⁴⁴ but the lower activation energy derived from chemical vapor deposition studies, 20 kcal/mol,^{12,16} is used in order to include the autocatalytic nature of the decomposition.

The specifics of the competition between dissociation and desorption of CO are of interest here, but few detailed kinetics studies of them are available. Since the chemistry of CO adsorption and dissociation on Cr, Mo, and W is similar,¹⁷⁻¹⁹ data from studies of an individual system, CO on W(110), are taken to be representative of all three metals.^{45,46} This is not an ideal situation, but for the purposes of the present model it is a reasonable approximation. Investigation of the kinetics of desorption of molecular CO from W(110) provides coverage-dependent Arrhenius parameters.⁴⁵ The *A* factor is reported to be $1 \times 10^{11} \text{ s}^{-1}$ and the activation energy, 20.5 kcal/mol.⁴⁵ Because of the coverage dependence, the *A* factor is too low for a typical primary first-order desorption step,^{42,47} and a value of $1.2 \times 10^{15} \text{ s}^{-1}$ has been substituted. As trial simulations progressed, it became evident that even with a higher *A* factor the desorption of CO was not sufficiently fast: molecular CO was found to accumulate on the surface even at a temperature well above that where kinetics studies show it to have either dissociated or completely desorbed.^{17-19,45,46} Consequently, the activation energy was lowered until accumulation occurred only at about 325 K or below; a value of 15 kcal/mol appeared to be optimum. The lower value may not be physically unreasonable since the instantaneous local coverage of CO under film growth conditions is likely to be high, and the average desorption energy might decrease as a result.⁴⁵ The dissociation step, (5), is also investigated in ref 45, yielding an *A* factor of $2 \times 10^{21} \text{ s}^{-1}$ and an activation energy of 5 kcal/mol. This rate constant was found to be too small to permit any CO dissociation, so it was increased as follows. The *A* factor as reported is too low for a primary first-order CO dissociation step, which involves (at least in the case of Cr) a four-center transition state.¹⁷ A reasonable value, taken from unimolecular cyclization reactions,⁴⁷ is 10^{10} s^{-1} . Even with this increase the rate of dissociation, known to be maximum around 300–400 K,⁴⁵ did not have the correct temperature dependence. It was found that a value of 9.5 kcal/mol gave much more reasonable results. The reason for the nearly 5 kcal/mol discrepancy with experiment is not entirely clear. From the discussion of the kinetics studies

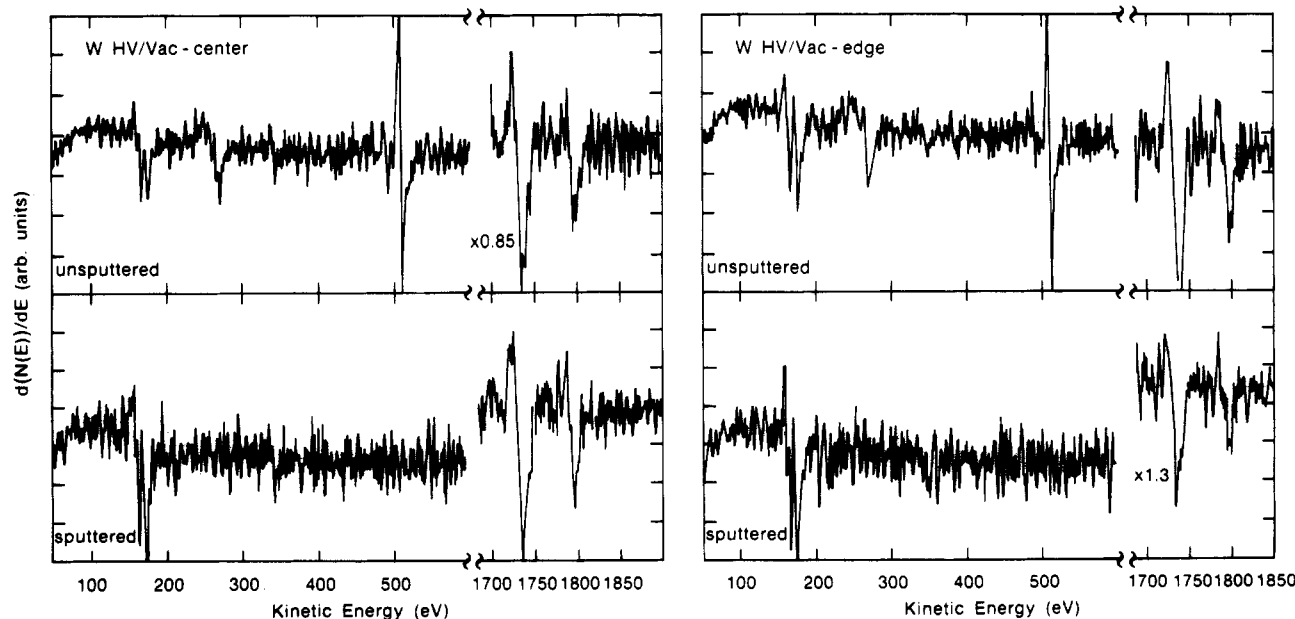


Figure 14. Auger survey spectra of an HV/vac W film deposited using a 2.80 MW/cm² beam for 90 s.

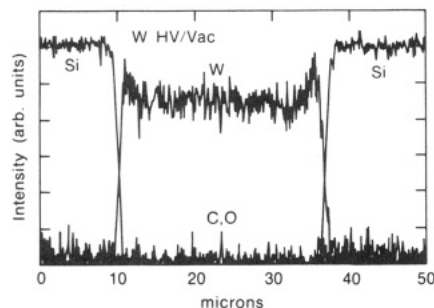


Figure 15. Auger linescan of a W film deposited under HV/vac conditions after sputtering for 20 min (2.80 MW/cm^2 , 30 s).

presented in ref 45, it is evident that the composition between desorption and dissociation over the temperature range of the measurements, leading to continuous changes in coverage and site availability, complicates the analysis of the kinetics considerably. The dissociation rate constant derived from the data was judged to be remarkably low, with a very weak temperature dependence (activation energy).⁴⁵ Finally, kinetic parameters measured for recombinative desorption of C and O, reaction 6, are taken to be $1.2 \times 10^{12} \text{ s}^{-1}$ and 69.5 kcal/mol ⁴⁶ and are used without adjustment.

All kinetics simulations are carried out using MSIMPC,⁴⁸ a stochastic mechanism simulator of a type described more fully elsewhere.^{33b,48} The reaction temperature is held constant for each simulation (representing chemistry at a particular radial position on the film surface), and concentration vs time curves for all reactants and products are calculated. Deposition rates and carbon concentrations in the metal films are shown in Table V for temperatures from 325 to 1000 K. The overall rate of deposition is too high by about an order of magnitude above 600 K, indicating that the $\text{M}(\text{CO})_6$ desorption rate is too low. No attempt has been made to optimize the kinetics of precursor adsorption and dissociation because of the obvious crudeness of the model. Nonetheless, the general agreement between the temperature range where the carbon content is maximum and the results of the comparison between film composition profiles and temperature profile simulations (Figure 16) indicates that the part of the mechanism describing CO chemistry is reasonably realistic. (Please see note added in proof.)

Discussion

Spatially resolved compositions measured for thin Cr, Mo, and W films deposited from the hexacarbonyls using CW visible laser

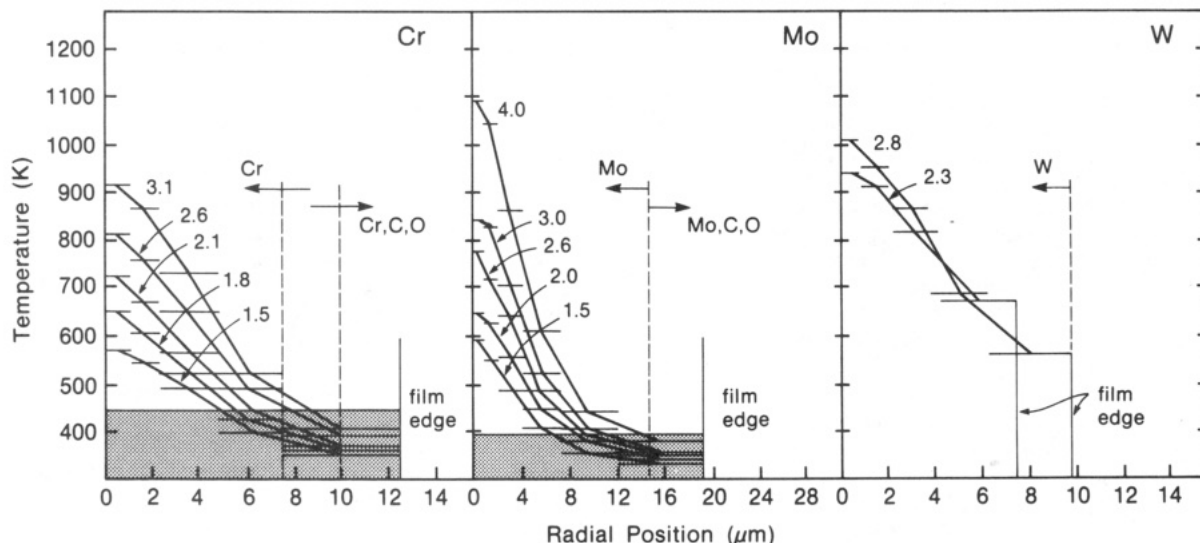


Figure 16. Simulated temperature profiles for Cr, Mo, and W films on Si substrates resulting from CW visible laser heating. The film geometries are $2.75\text{-}\mu\text{m}$ -thick disks, with diameters as shown on each panel of the figure (note the change in scale for Mo). The laser spot diameter is $10 \mu\text{m}$ ($1/e^2$), centered on the disks. The incident power densities, in MW/cm^2 , are indicated for each profile. The widths of the cells used in the calculations are shown as horizontal lines, in μm . The radial location of the transition from clean to contaminated material is marked for Mo and Cr. The surface temperature range where deposition of contaminated metal is expected is indicated by the shaded regions in the two panels.

TABLE V: Simulated Growth Rates and Carbon Concentrations

temp (K)	carbon/metal	rate (layer/s)	temp (K)	carbon/metal	rate (layer/s)
325	0 ^a	19	600	0.007	6825
350	0.5	45	700	0.005	17586
400	0.11	168	800	0.003	33719
450	0.01	683	900	0	56451
500	0.007	1812	1000	0	82710

^aNo CO dissociation occurred at this temperature.

TABLE VI: Summary of Approximate Film Compositions (HV/vac)

metal	515 nm		257 nm ^a	
	surface	bulk	surface	bulk
chromium				
center	CrCO	Cr	CrCO ₂	CrCO
edge	CrCO	Cr _{0.3} O _x ^b	CrCO ₂	CrCO
off spot	CrC ₂ O ₂ ^c		CrC ₂ O ₂	
interface		CrC _{0.5} O _{0.7}		
molybdenum				
center	MoC _{1.5} O	Mo	MoC ₂ O	MoC ₂ O _x ^d
edge	MoC ₂ O	MoC _{0.3} O _x ^d	MoC ₂ O	MoC ₂ O _x ^d
off spot	MoCO _{1.5}	MoCO _x ^d	MoC ₂ O	
interface		MoC _{0.5} O _x ^d		
tungsten				
center	WC _{0.5} O _{0.5}	W	WC _{0.5} O _{0.5}	WC _{0.5} O _x ^d
edge	WC _{0.5} O _{0.5}	W	WC _{0.5} O _{0.5}	WC _{0.5} O _x ^d
off spot	WCO		WC _{0.5} O _{0.5}	
interface		W		

^aData taken from ref 25. ^bOxygen stoichiometry affected by background gas contamination. ^cVisible laser-deposited off-spot material has somewhat more C and O than UV laser-deposited off-spot material, although they have the same composition within error limits ^dOxygen stoichiometry is low because of reductive sputtering.

excitation show that a range of materials are obtained. Approximate stoichiometries are summarized for vacuum-transferred films in Table VI, along with similar data obtained for films deposited by low-power UV laser irradiation (i.e., near-room temperature surface decomposition of coordinatively unsaturated metal carbonyls). It is evident that the relative amount of carbon and oxygen contamination depends on both the local temperature and the composition of the underlying material, with dynamically increasing purity as the film surface becomes more metallic and/or hotter. Studies of LCVD and $\text{Cr}(\text{CO})_6$ by molecular beam mass spectrometry are consistent with this result, showing clearly that

there are two film growth regimes connected by an abrupt transition.⁴³ Thermal and mechanistic modeling indicate that the minimum temperature for deposition of clean metal on clean metal is ≤ 450 K. The lack of incorporation of C and O is attributable to efficient desorption of CO from the metal surface. The presence of substantial thicknesses of heavily contaminated Cr and Mo at the edges and near the substrate interface, however, provides evidence that the ability of metal oxycarbide films to dissociate CO is greater than that of pure metal over a wide temperature range. The lack of impurities in the same regions of the W films indicates that the overall hexacarbonyl and CO reaction kinetics on the three metals are not identical. In this section some detailed aspects of these results are explored to obtain insight to characteristics of the growth process.

Nucleation Chemistry and Growth of Contaminated Films. Reliable initiation of growth from the hexacarbonyls requires the presence of a metal oxycarbide layer at the surface,^{4,16} indicating that dissociative chemisorption of the metal hexacarbonyl occurs more readily on this material than on the native oxide of silicon. This result is strikingly similar to observations of Mo hexacarbonyl loading efficiencies in preparation of catalysts on alumina or silica with various initial coverages of hydroxyl groups.⁴⁹⁻⁵¹ Dissociative chemisorption of $\text{Mo}(\text{CO})_6$ to form $\text{Mo}(\text{CO})_5$ occurs at room temperature on dehydroxylated or partly dehydroxylated alumina surfaces. This reaction has been attributed to the abundance of Lewis acid and Lewis base sites available.⁵² In contrast, silica is only weakly basic,⁵³ and the reactivity of the hexacarbonyls with it is relatively low.⁵⁰ At higher temperatures (600–800 K), the Mo carbonyl complexes decompose to form oxidized metal containing about 0.3 C/Mo.⁵⁴ Heating to 950 K is required to remove most of the carbon. The average Mo oxidation state on partly dehydroxylated alumina is 4 and that on dehydroxylated alumina is 0.3, consisting of clusters of Mo^0 on divalent molybdenum.⁵⁴ The metal state on silica is similar to that on dehydroxylated alumina.⁵¹ Although data for W and Cr are fewer because of the lower activities of catalysts made from them, several studies indicate that the surface reactions of tungsten and chromium hexacarbonyls on silica and alumina supports are similar to those of molybdenum.^{49-51,55}

The supported catalyst data indicate that a surface with strongly acidic and basic sites will dissociate metal hexacarbonyls readily and that below 950 K the material which is formed contains a mixture of oxidized and unoxidized metal and some carbon. Similarly, when the hexacarbonyls are used to grow films, it is found that decomposition on a preexisting metal oxycarbide layer (off-spot material) occurs much more readily than on the silicon dioxide surface and that the stoichiometry of the initial layer formed (see interfacial layer compositions in Table VI) is close to that of dehydroxylated alumina-supported catalyst material.⁵⁴ These observations suggest that the metal oxycarbide surfaces formed during film growth may have significant Lewis acid and base character. If so, growth of an oxycarbide film can be sustained by continual impingement and dissociation of precursor molecules onto the surface. This is a critical point: according to studies in UHV of CO and W hexacarbonyl decomposition on metal surfaces,^{17-19,22} preexisting coverages of C and O serve to inhibit dissociation of both molecules. If these observations were applicable to metal oxycarbide surfaces, it is clear that C and O concentrations should be limited to a total of about half a monolayer everywhere, instead of the much higher quantities observed experimentally.²⁵ In addition, appreciable film growth would be expected only on pure metal surfaces. The fact that significant dissociation levels are observed even on remote areas of the substrate provides evidence that the metal oxycarbide surfaces are quite reactive.

The commonality in chemistry between catalyst formation and activity and film deposition from the group VI hexacarbonyls, which to our knowledge has not been considered previously, suggests that the catalysis literature may be used to explore some details of nucleation and contaminated film growth in LCVD. We wish to stress that the present experiments are far from proving that this line of reasoning is valid; however, we believe that dis-

ussion of similarities and differences may prove useful in formulating experimental approaches to understanding nucleation in CVD systems in general.

The role of Lewis acid and base surface sites in promoting metal–CO and CO bond dissociation has been discussed. It has been suggested that oxide sites (Lewis bases) on alumina surfaces cause isomerization of the surface carbonyl intermediates and labilization of cis metal–CO linkages via interaction between the surface oxygen and the carbonyl carbon.⁵² Similarly, such surfaces can facilitate CO adsorption in a parallel rather than a perpendicular geometry.^{52,56} For example, the bonding geometry of CO on Cr_2O_3 ⁵⁶ is with the molecular axis parallel to the plane of the surface, allowing interaction of C and O with surface O and Cr sites. The parallel orientation allows substantial charge transfer from basic sites to CO, weakening the CO bond and promoting dissociation if it is kinetically accessible.^{57,59} It is possible that the ability of the metal oxycarbides to dissociate CO during film growth is linked to the Fischer–Tropsch activity of metal oxide and carbide catalysts.^{49,60-63} In this regard, the catalytic activity for CO hydrogenation is $\text{Mo carbide} > \text{Mo} > \text{MoO}_2 > \text{MoO}_3$ ⁶¹ and $\text{WC} > \text{W}_2\text{C} > \text{W}$,⁶³ suggesting that the presence of carbon increases the reactivity of the metal. Although whether dissociation of CO occurs before or after hydrogenation is not known, it has been suggested that the more metal-rich tungsten carbide tends to promote dissociation,⁶³ as do Lewis bases.⁵⁷

Additional parallels between nucleation and catalysis chemistry in the metal hexacarbonyls are found in the propensity for Mo-containing films to be enriched in carbon relative to oxygen (Tables II, III, and VI), signaling that CO_2 is a significant desorption product. Although rather little CO_2 is formed during thermal decomposition of supported Cr, Mo, and W hexacarbonyls in He,⁵¹ catalytic hydrogenation of CO over Mo_2C ,⁶² MoO_2/C , and $\text{Mo}_2\text{C}/\text{C}$ catalysts⁶⁰ produces copious amounts of CO_2 . Similarly, CO_2 is produced over WC and W_2C catalysts, but in lower quantities.⁶³ As hydrogen partial pressure decreases, the rate of CO_2 formation on Mo catalysts increases significantly, while it is independent of hydrogen on W_2C . In the limit of no hydrogen, these trends are compatible with metal–carbon–oxygen ratios obtained during deposition of contaminated films (especially off-spot material). The closer resemblance of CO_2 formation rates in film growth to carbide catalysts than supported metal carbonyls may be due to oxygen depletion in the latter system. In film growth, as in flowing catalytic reactors, CO dosing rates are high and surface oxygen is renewed through precursor decomposition.

Although Mo-containing catalysts are very similar in composition to W-containing ones, as are their catalytic properties, the films grown by LCVD from Mo and W hexacarbonyls are very different. Mo shows a range of contamination levels, both interfacial and peripheral, while W has impurity levels below the Auger detection limit excepting the off-spot material. Cr is similar to Mo. The reasons for these differences may be attributable to a simple kinetic effect. Figure 16 and the laser power density requirements provide evidence that much higher surface temperatures are required for W than for Mo and Cr growth. This is due to part to the lower vapor pressure of $\text{W}(\text{CO})_6$ which leads to a lower dissociation rate. (Phenomenological activation energies for surface dissociation are about the same for the three metals.^{12,16}) Such high temperatures may be sufficient to ensure dominance of CO desorption and clean W growth from the earliest times. For Mo and Cr, on the other hand, film growth occurs over a much wider range in temperatures and CO dissociation is kinetically important. The balance between dissociation and desorption is quite sensitive to local temperature and film surface composition. The observation of progressively increasing metal content in the center regions of Mo and Cr films suggests that sites which can easily dissociate CO are reduced in number as new material is added.

Although the chemical kinetics remain to be established and quantified, the implications of this line of reasoning for film purity are clear. An increase in CO dissociation rate obtained by simply lowering the activation energy by 1–2 kcal/mol can significantly affect the competition between dissociation and desorption during

deposition. Indeed, simulations of (1)–(6) predict that such a decrease raises the minimum temperature for obtaining clean metal to over 700 K.

As a final point, it is interesting to note that trends in evolution of film diameters (Film Characterization section) are remarkably consistent with relative activities of catalysts formed from the metal hexacarbonyls. Although the vapor pressure of the Mo carbonyl is only 2.5 times higher than that of tungsten carbonyl, and the initial surface temperature distributions on Mo- and W-containing off-spot material are likely to be similar, the Mo films at 1 s are 5–6 times larger than the W films. Indeed, the Fischer–Tropsch catalytic activity of $\text{Mo}(\text{CO})_6/\text{Al}_2\text{O}_3$ is appreciably higher than $\text{W}(\text{CO})_6/\text{Al}_2\text{O}_3$.⁵⁴ Mo and Cr films are similar in size at early times, although the vapor pressure of Mo carbonyl is only one-third that of Cr, suggesting that the Mo oxycarbide surface is more reactive than that of Cr as well. Few studies of catalytic activity of supported chromium carbonyl catalysts have been reported,⁴⁹ however, and their reactivity is deemed to be low. The reason for this is not clear, but it may have to do with difficulties in controlling the oxidation of Cr during catalyst preparation or with rapid poisoning during reaction. Under high-vacuum film growth conditions the surface is continually renewed and extraneous oxidation is minimized, however, allowing substantial CO and hexacarbonyl dissociation to occur. It is worth considering that the propensity to form rings or disks at early times and generally complex film topographies at later times may also be related to the metal oxycarbide surface reactivity. Such structures are commonly observed in LCVD and have been attributed to a variety of effects including mass transport and temperature-dependent sticking probabilities.^{64,65} Little is known about film growth chemistry in LCVD, however, and the possible importance of chemical reactivity in determining local growth rates and thus film topography has not been considered.

The discussion of reactivity presented in this section suggests that the surface chemistry occurring at the early stages of film growth and at the perimeter of the films is substantially more complex than the simple mechanism proposed for steady-state deposition of clean metal. It is obviously premature to consider formulation of a model for nucleation; however, experiments connecting surface composition and volatile product formation which are currently in progress in our laboratories may eventually allow a more quantitative description of the kinetics to be made.

Growth of Clean Metal Films: Reactions of CO. Once the surface composition of the film centers has evolved to pure metal, simulations of temperature-dependent film deposition and correlation of radial composition and temperature profiles can be used to devise a simple mechanism for steady-state growth. The most significant finding from the model calculations is that the competition between CO dissociation and desorption, a primary factor in controlling film purity, overwhelmingly favors desorption above about 450 K. Since few C and O atoms are present on the surface, high-temperature recombinative desorption is kinetically insignificant, and the desorption process is primarily molecular. Analyses of desorbing CO confirm this result, showing no evidence of increased desorption rates at high temperature.⁴³ Accordingly, it appears that the metal hexacarbonyls are very good precursors for low-temperature deposition as long as conditions leading to metal oxycarbide formation are avoided or when thin contaminated interfacial layers can be tolerated. The present results are in disagreement with previous studies, which consistently point to a requirement for >800 K to obtain clean films.^{12–16,20,22}

As described in the Introduction, temperature-programmed reaction studies of Mo and W hexacarbonyls have been carried out in ultrahigh vacuum on metal and silicon surfaces.^{20–23} The motivation for these experiments has been to learn how decomposition kinetics of the precursors might effect the purity of films grown both thermally and photochemically. The results show that there is extensive dissociation at low temperatures (about 300 K) leading to significant, thermally stable coverages of metal, oxygen, and carbon atoms.^{20–23} This has prompted the suggestion that formation of metal oxycarbides is inevitable during film growth unless extremely high surface temperatures are maintained.²² The

discrepancy between the temperature-programmed reaction data and the present results can be understood by considering the evolution of surface adsorbates during a temperature ramp. The metal hexacarbonyl is typically dosed onto a substrate held at liquid nitrogen temperature; then the crystal is warmed to 1000 K or so. As the surface temperature reaches about 300 K, extensive desorption or dissociation of both precursor and CO occurs. The atomic species formed do not react further until the upper range of the surface temperature ramp is reached because their mobility is low.⁶⁶ In contrast, during LCVD the temperature near illuminated regions of the surface is maintained well above room temperature, with a distribution likely to be essentially constant once the optical and thermal properties of the system have stabilized.⁶⁷ The CO desorption rate is sufficiently high over most of the film surface that dissociation is insignificant. Only the film edges approach room temperature, where relative CO dissociation rates are highest, and they can indeed contain significant amounts of impurities. It is evident from these considerations that the use of a ramp in the temperature-programmed reaction experiments has introduced a significant kinetic bias by inducing so much decomposition early on. The chemical reactions observed in those studies are of interest but are not typical of isothermal film growth.

Although pure metal can be deposited by LCVD from the hexacarbonyls, similar success has not been achieved in CVD except at very high temperatures.^{12–16} It is not clear why such different results have been obtained in nominally similar systems. Factors favoring contaminant incorporation in CVD may include introduction of trace impurities through carrier gases and high system background pressures or perhaps more subtle effects due to gas temperature, flow rates, or reactor geometry. Experiments designed to address this question are in progress.

Interesting questions also arise concerning the steady-state composition of the film surface during growth. The simulations and discussion thus far do not presume anything concerning details of hexacarbonyl adsorption and dissociation or CO binding sites. Although salient features of the experimental data can be understood purely in terms of CO reactivity, evidence exists that there may be considerable additional complexity. CO recombinative desorption kinetics are known to be fast at much lower temperatures when C and O coverages are high.⁶⁸ This pathway may compete with direct desorption if film growth rates are fast and CO dissociation rates are higher than estimated. On the other hand, if the CO ligands remain associated with well-defined complexes, crowding may inhibit reorientation and dissociation, and direct desorption may always dominate. Although temperature-programmed reaction studies had not found evidence for such complexes at elevated temperatures, in situ molecular beam mass spectrometric measurements suggest that partly carbonylated metal intermediates are indeed present on the surface during Cr deposition during both growth and pregrowth regimes.⁴³ Investigations of the chemical nature of hexacarbonyl catalysts show that unsaturated Mo and W carbonyls are also formed on alumina and silica supports.⁴⁹ Thermal reactions of carbonyl complexes may not be the only channels which are open, adding further complication. Time-of-flight measurements of desorbing CO hint that photolabile intermediates may be present on the surface during LCVD.⁴³ If stimulated desorption of CO does indeed occur, it cannot account in full for the radial composition profiles since the illuminated area is much smaller than the clean region of the films. Nonetheless, the kinetic consequences of such pathways, particularly for film nucleation, should be investigated.

Reactivity of Deposited Films. In addition to providing information on film nucleation and growth chemistry, the present studies enable assessment of the susceptibility to contamination of materials deposited from the hexacarbonyls. Sources of contaminants include background gases, the metal hexacarbonyls, and handling in air.

Comparison of the thermally deposited LV/air and HV/air films shows that when a high-base-pressure cell is used the film bulks and edges are free of carbon, and the oxygen levels are markedly higher. The overall oxygen content is lower than that found for the photochemically deposited films, however.²⁵ This

may be attributable to elevated temperatures and lower sticking probabilities, to inherent differences in reactivity of essentially clean metal vs a metal oxycarbide as is formed in photodeposition, or to the higher thermal deposition rate.

Although regions of the films are found to be pure, the metal is in fact encapsulated by significant quantities of oxycarbides of varying stoichiometries (see Table VI). It is likely that this material is formed after deposition, since the film surfaces remain in contact with precursor gases and newly formed CO. Continuing adsorption and reaction under ambient conditions are not surprising, given the ability of Mo,²⁰ W,²² and Cr⁴³ to dissociate the metal hexacarbonyls. If the resulting surface has oxycarbide (Lewis acid and base) character, then it can also continue to dissociate precursor molecules.⁴⁹

It is interesting to note that the surface material can be similar in composition to that obtained by photochemical deposition from the same precursors, suggesting that some common reaction pathways may be operant once a metal hexacarbonyl has lost one or more CO ligands. There are likely to be significant structural differences between the materials, however. Room-temperature photochemical deposition results in oxycarbide films which are extremely air sensitive.²⁵ Exposure to oxygen-containing gases results in oxidation throughout the thickness of the films, segregation of carbon to the film surfaces, and desorption of carbon-containing products, presumably CO and CO₂. In contrast, laser thermal deposition results in film surfaces and bulks which are much more air stable: HV/air and HV/vac films are quite close in composition. This is most likely due to a higher compactness of the thermally deposited films. Material photochemically deposited by a polarized laser beam is deeply corrugated, resembling an ear of corn. It appears that this structure and the lower density expected of films grown under conditions of low surface mobility⁶⁹ are most detrimental to their chemical stability. The disorder imposed by the high levels of impurities⁶⁹ is evidently of less importance, as judged from the minimal oxidation of contaminated edges of thermally grown films.

Conclusions

A systematic investigation of thin Cr, Mo, and W films deposited by laser chemical vapor deposition from the hexacarbonyls has been performed. The study includes spatially resolved elemental analyses of films deposited under a range of conditions and modeling of temperature profiles and surface reaction kinetics at steady state. The results show that very pure metal can be grown from these precursors despite the high reactivity of CO on early transition metal surfaces once a minimum temperature range (<450 K) has been exceeded and a metal-rich surface has been formed. Kinetics simulations reveal that the purity of the metal is attributable to the efficiency of CO desorption. Since CO dissociation is not competitive, desorption is molecular in character and not recombinative. Contaminated films are formed as well. Cr and Mo films show high levels of carbon and oxygen in remote, cooler areas of the substrate, at the edges of the films, and near the film-substrate interface. W films, on the other hand, are spatially homogeneous, with significant C and O concentrations only found far from heated locations. The sustained growth of contaminated material, the requirement for its presence to nucleate clean films, and its evolution from metal oxycarbide to metal are discussed in terms of the catalytic properties of Mo and W carbides and oxides and supported catalysts formed from the metal hexacarbonyls. Taken together, the composition data and the literature suggest that the metal oxycarbide surfaces can dissociate metal hexacarbonyls, and their ability to dissociate CO is greater than that of the corresponding clean metals at a given temperature. This serves to shift the CO reaction kinetics away from desorption.

The results reported here are in disagreement with conclusions drawn from temperature-programmed reaction and conventional chemical vapor deposition studies using the group VI metal hexacarbonyls. Those investigations indicate that temperatures above 800 K are required to obtain clean films because of CO dissociation on the film surface. The discrepancy between the present study and the temperature-programmed reaction exper-

iments is attributable to a kinetic bias introduced by use of a temperature ramp. It is also possible that kinetic conditions present at low surface coverages may also play a role in the accumulation of C and O: unless there is continuous precursor, dosing the system may always mimic nucleation and not steady-state growth. Conventional surface science techniques should be applied with caution to studies of chemical vapor deposition until the relevant kinetics are better understood. The inconsistency between LCVD and CVD results, on the other hand, remains to be explained.

Note Added in Proof. We have recently modified MSIMPC⁴⁸ to calculate temperature-programmed reaction mass spectra. We have used the code to simulate CO desorption during metal hexacarbonyl decomposition from steps 1-6 for comparison to experiments on W(CO)₆ on W(110).²² The qualitative agreement is quite good considering the crudeness of our mechanism, the main discrepancy being an underestimation of the molecular CO desorption rate between 200 and 300 K. The consistency of the simulations with both LCVD and temperature-programmed reaction data indicates that (1)-(6) provide a reasonable description of central elements of the reaction. We are currently working to refine our model to include coverage and bonding state effects.

Acknowledgment. We are grateful to Jorge Goitia for providing technical assistance, to W. D. Hinsberg for contributions to the development of the heat flow simulator, and to IBM East Fishkill for support of K.A.S. as a visiting scientist at IBM Almaden Research Center during the summer of 1990. K.A.S. thanks the National Science Foundation (Grant RII-8911281), the donors of the Petroleum Research Fund (administered by the American Chemical Society), and the Affirmative Action Faculty Development Program at San Jose State University for financial support. This work was performed under a joint study agreement between IBM and SJSU.

References and Notes

- (1) Lu, X.; Zhang, J.; Qui, M. *Thin Solid Films* **1991**, *196*, 95.
- (2) Petzhold, H.-C.; Putzar, R.; Weigmann, U.; Wilke, U. *Mater. Res. Soc. Symp. Proc.* **1988**, *101*, 75.
- (3) Nambu, Y.; Morishige, Y.; Kishida, S. *Appl. Phys. Lett.* **1990**, *56*, 2581.
- (4) Oprysko, M. M.; Beranek, M. W. *J. Vac. Sci. Technol. B* **1987**, *5*, 496.
- (5) Tonneau, D.; Auvart, G.; Pauleau, Y. *J. Phys., Colloq.* **1989**, *50*, C5-647.
- (6) Gilgen, H. H.; Cacouris, T.; Shaw, P. S.; Krchnavek, R. R.; Osgood, R. M. *Appl. Phys.* **1987**, *B42*, 55.
- (7) An excellent summary of this system has been given by: Herman, I. P. *Chem. Rev.* **1989**, *89*, 1323 and references therein.
- (8) Farkas, J.; Hamori, A.; Szabo, Z. *Proc. SPIE* **1990**, *1264*, 362.
- (9) Yokoyama, H.; Uesugi, F.; Kishida, S.; Washio, K. *Appl. Phys.* **1985**, *A37*, 25.
- (10) Yokoyama, H.; Kishida, S.; Washio, K. *Appl. Phys. Lett.* **1984**, *44*, 755.
- (11) Gray, H. B.; Beach, N. A. *J. Am. Chem. Soc.* **1963**, *85*, 2922.
- (12) Kaplan, L. H.; d'Heurle, F. M. *J. Electrochem. Soc.* **1970**, *117*, 693.
- (13) Thomas, L. K.; Chain, E. E. *Thin Solid Films* **1983**, *105*, 203.
- (14) Yous, B.; Robin, S.; Robin, J.; Donnadiou, A. *Thin Solid Films* **1985**, *130*, 181.
- (15) Carver, G. E. *Sol. Energy Mater.* **1979**, *1*, 357.
- (16) Kunz, R. R.; Mayer, T. M. *J. Vac. Sci. Technol.* **1988**, *B6*, 1557.
- (17) Shinn, N. D.; Madey, T. E. *J. Chem. Phys.* **1985**, *83*, 5928. Shinn, N. D. *Langmuir* **1988**, *4*, 289.
- (18) Ko, E. I.; Madix, R. J. *Surf. Sci.* **1981**, *109*, 221.
- (19) Benziger, J. R.; Ko, E. I.; Madix, R. J. *J. Catal.* **1978**, *54*, 414.
- (20) Cho, C. C.; Bernasek, S. L. *J. Appl. Phys.* **1989**, *65*, 3035.
- (21) Gluck, N. S.; Ying, Z.; Bartosch, C. E.; Ho, W. *J. Chem. Phys.* **1987**, *86*, 4957.
- (22) Flitsch, F. A.; Swanson, J. R.; Friend, C. M. *Surf. Sci.* **1991**, *245*, 85.
- (23) Swanson, J. R.; Flitsch, F. A.; Friend, C. M. *Surf. Sci.* **1990**, *226*, 147.
- (24) A preliminary report of Cr, Mo, and W LCVD from the hexacarbonyls has been published in: Singmaster, K. A.; Houle, F. A. *Mater. Res. Soc. Symp. Proc.* **1991**, *201*, 209.
- (25) Singmaster, K. A.; Houle, F. A.; Wilson, R. J. *J. Phys. Chem.* **1990**, *94*, 6864.
- (26) Preston, J. S.; van Driel, H. M.; Sipe, J. E. *Phys. Rev. Lett.* **1987**, *58*, 69.
- (27) Davis, L. E.; MacDonald, N. C.; Palmberg, P.; Reich, G. E.; Weber, R. E. *Handbook of Auger Electron Spectroscopy*, 2nd ed.; Perkin Elmer Corp.: Eden Prairie, MN, 1978.
- (28) Kato, H.; Sakisaka, Y.; Miyano, T.; Kamei, K.; Nishijima, M.; Onchi, M. *Surf. Sci.* **1982**, *114*, 96.

- (29) Grant, J. T.; Haas, T. W. *Surf. Sci.* **1971**, *24*, 332.
 (30) Lesiak, B.; Mrozek, P.; Jablonski, A.; Joswik, A. *Surf. Interface Anal.* **1986**, *8*, 121.
 (31) Carslaw, H. S.; Jaeger, J. C. *Conduction of Heat in Solids*, 2nd ed.; Oxford University Press: Oxford, 1986.
 (32) Houle, F. A.; Hinsberg, W. D. To be submitted for publication.
 (33) (a) Gillespie, D. T. *J. Comput. Phys.* **1976**, *22*, 403. Turner, J. S. *J. Phys. Chem.* **1977**, *81*, 2379. (b) Bunker, D. L.; Garrett, B.; Kleindeinst, T.; Long, III, G. S. *Combust. Flame* **1974**, *23*, 373.
 (34) Lariokapis, E.; Raptis, Y. S. *J. Appl. Phys.* **1985**, *57*, 5123.
 (35) Hicks, J. M.; Urbach, L. E.; Plummer, E. W.; Dai, H. L. *Phys. Rev. Lett.* **1988**, *61*, 2588.
 (36) Touloukian, Y. S.; Powell, R. W.; Ho, C. Y.; Klemens, P. G. *Thermophysical Properties of Matter*; IFI/Plenum: New York, 1970; Vol. 1.
 (37) Touloukian, Y. S.; Buyco, E. H. *Thermophysical Properties of Matter*; IFI/Plenum: New York, 1970; Vol. 4.
 (38) Ho, C. Y.; Powell, R. W.; Liley, P. E. *J. Phys. Chem. Ref. Data* **1974**, *3* (Suppl. 1), I-588.
 (39) Wicks, C. E.; Block, F. E. *Thermodynamic Properties of 65 Elements—their oxides, halides, carbides and nitrides*, Bulletin 605; U.S. Bureau of Mines: Washington, DC, 1963, p 103.
 (40) Palik, E. D., Ed. *Handbook of Optical Constants of Solids*; Academic: Orlando, 1985.
 (41) Weaver, J. H.; Kraffka, C.; Lynch, D. W.; Koch, E. E. *Physics Data: Optical Properties of Metals*, 18-1; Fachinformationzentrum Energie, Physik, Mathematik GmbH: Karlsruhe, 1981.
 (42) Adamson, A. W. *Physical Chemistry of Surfaces*, 4th ed.; Wiley: New York, 1982; Chapters 16 and 17.
 (43) Houle, F. A.; Yeh, L. I. *J. Phys. Chem.* **1992**, *96*, 2691.
 (44) Lewis, K. E.; Golden, D. M.; Smith, G. P. *J. Am. Chem. Soc.* **1984**, *106*, 3905.
 (45) Umbach, E.; Menzel, D. *Surf. Sci.* **1983**, *135*, 199.
 (46) Kohrt, C.; Gomer, R. *Surf. Sci.* **1971**, *24*, 77.
 (47) Robinson, P. J.; Holbrook, K. A. *Unimolecular Reactions*; Wiley: London, 1972.
 (48) Hinsberg, W. D.; Houle, F. A., *MSIMPC v2.0—an Interactive Discrete Chemical Mechanism Simulator for the IBM PC*; Quantum Chemistry Program Exchange, Indiana University, 1991, Program QCMP-069.
 (49) Bailey, D. C.; Langer, S. H. *Chem. Rev.* **1981**, *81*, 109.
 (50) Brenner, A.; Burwell, R. L., Jr. *J. Catal.* **1978**, *52*, 364.
 (51) Brenner, A.; Hucul, D. A.; Hardwick, S. J. *Inorg. Chem.* **1979**, *18*, 1478.
 (52) Laniecki, M.; Burwell, R. L., Jr. *J. Colloid Interface Sci.* **1980**, *75*, 95.
 (53) Morrison, S. R. *The Chemical Physics of Surfaces*, 2nd ed.; Plenum: New York, 1990; Chapter 4.
 (54) Bowman, R. G.; Burwell, R. L., Jr. *J. Catal.* **1980**, *63*, 463.
 (55) Brenner, A.; Hucul, D. A. *J. Catal.* **1980**, *61*, 216.
 (56) Kuhlbeck, H.; Xu, C.; Dillmann, B.; Hassel, M.; Adam, B.; Ehrlich, D.; Wohlrab, S.; Freund, H.-J.; Ditzinger, U. A.; Neddermeyer, H.; Neuber, M.; Neumann, M. *Ber. Bunsen-Ges. Phys. Chem.* **1992**, *96*, 15.
 (57) Muetterties, E. L.; Stein, J. *Chem. Rev.* **1979**, *79*, 479.
 (58) Bell, A. T. *Catal. Rev.—Sci. Eng.* **1981**, *23*, 203.
 (59) Pavao, A. C.; Braga, M.; Taft, C. A.; Hammond, B. L.; Lester, W. A., Jr. *Phys. Rev.* **1991**, *B43*, 6962.
 (60) Bridgewater, A. J.; Burch, R.; Mitchell, P. C. H. *J. Catal.* **1982**, *78*, 116.
 (61) Saito, M.; Anderson, R. B. *J. Catal.* **1980**, *63*, 438.
 (62) Kojima, I.; Miyazaki, E. *J. Catal.* **1984**, *89*, 168.
 (63) Kojima, I.; Miyazaki, E.; Inoue, Y.; Yasumori, I. *Bull. Chem. Soc. Jpn.* **1985**, *58*, 611.
 (64) Skouby, D. C.; Jensen, K. F. *J. Appl. Phys.* **1988**, *63*, 198.
 (65) Moylan, C. R.; Baum, T. H.; Jones, C. R. *Appl. Phys.* **1986**, *A40*, 1 and references therein.
 (66) Chen, J.-R.; Gomer, R. *Surf. Sci.* **1979**, *81*, 589.
 (67) Houle, F. A. *Laser Chem.* **1988**, *9*, 107.
 (68) Viswanath, Y.; Schmidt, L. D. *J. Chem. Phys.* **1973**, *59*, 4184.
 (69) Neugebauer, C. A. *Phys. Thin Films* **1964**, *2*, 1.

Comparison of Chemical Schemes for Si Atomic Layer Epitaxy

S. M. Gates

IBM Research Division, T. J. Watson Research Center, Yorktown Heights, New York 10598

(Received: August 3, 1992)

Chemical schemes for Si atomic layer epitaxy (ALE) are discussed using a two-step sequence of reactions: (1) surface chlorination, using a chlorosilane molecule, and (2) reduction (Cl removal), using atomic H or a silane molecule. The schemes are compared in terms of equilibrium thermodynamics, to select the most promising schemes. All of the proposed processes based on atomic H are spontaneous (thermodynamically downhill). Two reactions using Si₂H₆ are endothermic, but may be thermally driven at useful Si-growth temperatures, due to a large, positive entropy change for the reaction.

I. Introduction

Thin-film growth using cycles of self-limiting adsorption steps, with resulting layer-by-layer growth, is known as atomic layer epitaxy (ALE).^{1,2} Extension of ALE from binary materials to elemental semiconductors such as Si or diamond is a research area of current interest. Concerning Si growth, motivations to develop this method are fine control over deposited film thickness, insensitivity of growth rate to changes in processing parameters, and the goal of depositing very abrupt "δ-doped" layers. Uniform growth rate over large areas is another useful feature of ALE. The possibility of layer-by-layer growth of single-element materials, such as Si and diamond, is also a fascinating challenge which is stimulating research in the surface chemistry of these materials. The only previous example of Si-film growth by ALE used self-limiting adsorption of Si₂H₆ at temperatures (*T*) below the H₂ desorption temperature, and rapid photothermal heating with an excimer laser pulse to desorb the surface hydrogen.³ It is not clear what chemical schemes will be most useful for *isothermal* Si ALE at low temperature.

First, we examine thermodynamics of example reactions from the ALE literature on the growth of binary materials. These example ALE schemes use reactions that are "downhill" ther-

modynamically (negative Δ*G*). Second, potential schemes for Si ALE using chlorosilanes and H/Cl exchange chemistry^{4,5} are compared with respect to equilibrium thermodynamics. Equilibrium is not reached in film-growth reactors, but the hypothetical equilibrium case serves as a qualitative guide in choosing facile reactions that are "downhill" thermodynamically. Also, a closed reactor for investigating ALE chemistries with the reactants and film allowed to reach equilibrium in each cycle has been recently discussed.⁶ Finally, Si reactions that are promising on the basis of thermodynamics are discussed with regard to other factors.

II. Thermodynamics of ALE Schemes

A. Tables of Thermodynamic Data. Tables I–IV summarize the equilibrium thermodynamics of the net reactions considered for ALE. The state labels are omitted from the reactions in all the tables, for simplicity. All reactants, and H₂ and HCl products, are gases. The remaining products are solids. Tabulations of standard thermodynamic functions^{7–9} were used to calculate Δ*H*⁰ and Δ*G*⁰, both at 300 K. Also, Δ*S*⁰ was calculated (not shown), and an estimate of Δ*G* at 775 K (est Δ*G*) was made *assuming* that Δ*H* is independent of *T*, using est Δ*G* = Δ*H*⁰ – (775 K × Δ*S*⁰).